

In-Situ Response of WC-Ni Composites under Compressive Load

J.W. PAGGETT, A.D. KRAWITZ, E.F. DRAKE, M.A.M. BOURKE, B. CLAUSEN, and D.W. BROWN

The *in-situ* strain response of WC-Ni cemented carbides (5, 10, and 20 wt pct Ni) to uniaxial compressive load was measured using neutron diffraction. Strain was measured in both phases parallel and transverse to the loading axis of cylindrical samples. Plasticity is observed in the Ni binder from the lowest levels of applied load. The plasticity occurs locally in the Ni phase, on the scale of the microstructure, and leads to continuous curvature of the WC-Ni stress-strain curves and significant toughness of the material. The plasticity results from the interaction of the thermal residual microstresses created during sample production with the applied macrostress. It also leads to anisotropic relaxation of the initial residual stress and the creation of a residual stress state with cylindrical symmetry in the material. This process was observed over three load-unload cycles. Analysis enables phase-specific stress strain curves to be constructed. Finally, strain distributions were observed through peak breadth responses.

DOI: 10.1007/s11661-007-9196-4

© The Minerals, Metals & Materials Society and ASM International 2007

I. INTRODUCTION

CEMENTED carbide composites are used in applications requiring high strength, wear resistance, and toughness, such as oil, gas, and mineral exploration and mining; high speed machining; and high-temperature dies.^[1] Their deformation, fracture, and fracture toughness, which are unusually high for such hard materials, have been the subject of interest for many years.^[2–9] The most widely used and studied system, WC-Co, has the complication of a strain-induced phase change of the (metastable) face-centered cubic Co phase to the stable hexagonal close-packed form during deformation. From the point of view of neutron scattering, it is a poor candidate for study because of the high absorption and weak scattering characteristics of the cobalt. For these reasons, the present study addresses the WC-Ni system. The main goals were to (1) understand the stress-strain response of cemented carbides, (2) observe the phase-specific response of these composites under load, (3) investigate the interaction between applied stress and thermal residual stress (TRS), and (4) gain insight into the origins of toughness in this class of materials. Similar results for WC-Co were also obtained^[10] and will be compared in a subsequent article.

Neutron diffraction enables relatively large volumes (about 1 cm³) of WC-Ni to be sampled due to the low absorption of neutrons by even the heavy element W and enables phase-specific data to be collected *in situ*. Use of a pulsed neutron source enables simultaneous collection of all peaks of diffracting planes with interplanar spacings from about 0.5 to 4.0 Å in both the axial and transverse directions. In this study, the *elastic* strain response was monitored in WC-Ni samples during uniaxial compressive loading and unloading. In addition, both the initial TRS (introduced because of differences in the coefficients of thermal expansion between WC and Ni during production) and the final residual stresses after loading were determined.

Previous experimental studies of the TRS in cemented carbides have shown that the *mean* stresses are compressive in the carbide and tensile in the binder and are considerable in magnitude.^[10–14] For example, results for WC-15.6 wt pct Ni were 1215 MPa for Ni and –496 MPa for WC.^[11] Also, when measured by neutron diffraction, they are independent of *sample* orientation due to the fact that many grains (binder) and particles (carbide) are sampled. As a result, they are sometimes termed “diffraction hydrostatic,” even though, at a microstructural level, point-to-point and directional variations are present. These variations are significant, as modeled using finite element methods.^[15] In the Ni, for which the average TRS is tensile, there are local regions of residual stress that range from tension values well above the mean to low compression (in narrow bands between WC particles). In the WC, for which the average TRS is compressive, there are local regions that range from compression well below the mean to low tension (normal to WC/Ni interfaces). These stress *distributions* are largely due to the angularity of the carbide grains.^[12] Changes in the stress distribution

J.W. PAGGETT, Postdoctoral Fellow, is with the Materials Science and Engineering Department, University of Michigan, Ann Arbor, MI 48109-2136, USA. A.D. KRAWITZ, Professor Emeritus, is with the Mechanical and Aerospace Engineering Department, University of Missouri, Columbia, MO 65211, USA. Contact e-mail: krawitza@missouri.edu. E.F. DRAKE, Director, Materials Technology, is with the ReedHycalog, Houston, TX 77252, USA. M.A.M. BOURKE, Technical Staff Member, Acting Group Leader, B. CLAUSEN and D.W. BROWN, Technical Staff Members, are with the Los Alamos National Laboratory, NM 87545, USA.

Manuscript submitted September 13, 2006.

Article published online July 3, 2007.

(actually, the strain variance) can, in principle, be monitored *via* changes in the breadth of individual diffraction peaks, as discussed in Section III.

II. EXPERIMENTAL

A. Samples

The samples were WC-Ni cemented carbides with 5, 10, and 20 wt pct nickel binder. Metallographic characterizations are shown in Table I. Contiguity is the ratio of particle-particle contact area to the total (particle-particle plus particle-binder) contact area. Samples were produced by liquid-phase sintering at approximately 1400 °C followed by hot isostatic pressing. They were ground and lapped to cylinders 12 mm in diameter by 28 mm in length.

B. Compressive Loading

The compressive load response was measured on the spectrometer for materials research at temperature and stress (SMARTS) at the Los Alamos Neutron Science Center (LANSCE).^[16] SMARTS is a time-of-flight instrument with detector banks at ± 90 deg, so that data can be simultaneously collected in the axial and transverse directions of a cylindrical sample. The diffraction patterns, covering a d -spacing range from about 0.5 to 4 Å and including both the WC and Ni phase peaks, were fit using Rietveld refinement.^[17] The average elastic phase strains due to loading were calculated from the changes in the lattice parameters from the initial unloaded values. Thus, SMARTS provides independent values for the elastic strain of each phase in both the axial and transverse directions, at each step of a load-unload sequence. Because the strains were referenced to the lattice parameters of the phases prior to loading, they do not include the initial thermal residual strains. Each sample was loaded through three complete cycles, in increments of 250 MPa, from 0 MPa down to –2000 MPa and back to 0 MPa. The samples were held for approximately 6 minutes at each load level while diffraction patterns were collected.

C. Diffraction Stress Measurements

Measurements of the TRS on samples in their as-produced (unloaded) states were made on the Missouri University residual stress instrument (MURSI) at the Missouri University Research Reactor (MURR)^[18]

Table I. Sample Characterization

Property	WC-5 Wt Pct Ni	WC-10 Wt Pct Ni	WC-20 Wt Pct Ni
Volume pct Ni	7.3	15.9	27.6
WC particle size (μm)	1.14	1.17	0.93
Binder MFP (μm)	0.60	0.84	0.80
Contiguity	0.67	0.48	0.45
Hardness (Rockwell A)	90.9	88.6	83.9
Density (g/cm^3)	15.13	14.56	13.68

using a neutron wavelength $\lambda = 1.6549$ Å. Strain is determined from the shift in the position of a single peak with respect to an unstrained reference sample. From Bragg's law, $\lambda = 2d \sin \theta$, where λ is wavelength, d is interplanar spacing, and θ is the diffraction angle from the sample, the strain, ε , can be obtained using $\varepsilon = (d_{\text{sample}} - d_0)/d_0$, where d_{sample} and d_0 are the interplanar spacings in the sample and a stress-free reference standard, respectively. The relationship between Bragg's law and time-of-flight diffraction is

$$\lambda = 2d \sin \theta = ht/mL \quad [1]$$

where h is Planck's constant; t is the time-of-flight of the neutron; m is the rest mass of a neutron; and L is the source-to-detector distance, *i.e.*, the distance traveled by the neutron. The volume-averaged stress is then obtained from

$$\sigma = \frac{E}{1 - 2\nu} \varepsilon \quad [2]$$

where σ is the stress, E is Young's modulus, and ν is Poisson's ratio. For these measurements, the WC 201 peak was used and the unstrained reference sample was WC powder. Equation [2] assumes that the average TRS is the same in all directions (prior to loading), as has been shown previously for this class of material.^[19] Due to the effect solubility of W and C in Ni upon sintering on the cell parameter of Ni, an independent measurement of the initial Ni TRS cannot be made, although changes that occur upon loading can be accurately measured. Thus, the counterbalancing TRS in the Ni phase was calculated from the TRS in the WC phase using force balance considerations for microstress states.^[20,21]

$$(1 - f)\sigma_{\text{WC}} + f\sigma_{\text{Ni}} = 0 \quad [3]$$

where f is the volume fraction of Ni in the sample, σ_{WC} is the TRS in the WC phase, and σ_{Ni} is the TRS in the Ni phase.

Changes in residual stress after the three load cycles were measured in two ways: (1) using the initial and final data points on SMARTS and (2) using the procedure described previously on MURSI. On MURSI, the WC 201 and Ni 311 peaks were measured independently in both the axial and transverse directions, and the reference values were the peak positions in as-produced, but unloaded, samples. The final residual stress after loading was then found by adding the starting TRS to the measured change in residual stress after loading is complete. Results from these two approaches were in agreement within experimental errors.

The mechanical properties used for the WC 201 and Ni 311 lattice planes, as well as the macroscopic values,

Table II. Mechanical Properties Used for the WC 201 and Ni 311 Lattice Planes

Phase	E (GPa)	ν
WC 201	692	0.25
Ni 311	198	0.32

are shown in Table II. These values were calculated using the ISODEC program^[22] and elastic constants for Ni^[23] and WC.^[11] The macroscopic (polycrystalline) values were also calculated using ISODEC.

III. RESULTS AND DISCUSSION

A. Initial TRS

The mean TRS values in the samples prior to loading are shown in Table III. As seen in previous studies (*e.g.*, References 11 and 24), the residual thermal microstress in the Ni phase exceeds 2 GPa for all three compositions. The values of residual stress for both phases in the WC-10 pct Ni sample seem lower than expected compared to the other samples. The microstructure for this sample contained a number of very large WC grains, which serves to lower constraint in the material and reduce the TRS.

The magnitude of the binder stresses is 2 to 3 GPa, far greater than bulk Ni can support even when containing W and C in solution. This indicates a significant hydrostatic component and constraint by the hard carbide particles.^[25,26] It has been shown that the TRS is a strong function of WC particle size, for fixed composition and processing.^[24] As the particle size becomes finer, the binder constraint increases resulting in higher mean TRS values.

B. Axial and Transverse Response to Compression during the First Load-Unload Cycle

The responses for the 5, 10, and 20 pct Ni samples are shown in Figures 1 through 3. The errors for the measured strains are indicated in the figure captions; they are small. The stress-strain responses are continuously curved virtually from the onset of load. This is most pronounced in the macroscopic responses (total strain in the axial direction), shown in Figures 1(a), 2(a), 3(a), and 3(b), which are continuously curved, but is present in the applied stress-elastic phase strain responses as well, particularly for the Ni phase (Figures 1 through 3). This indicates plasticity from the earliest loads, as previously observed in WC-Co (in both tension and compression)^[10,27,28] and WC-Ni (compression).^[29] The deviation from linearity is greater in WC-Ni because Ni is a more ductile binder. The strain values at the maximum compressive stress of -2000 MPa for the first load cycle are

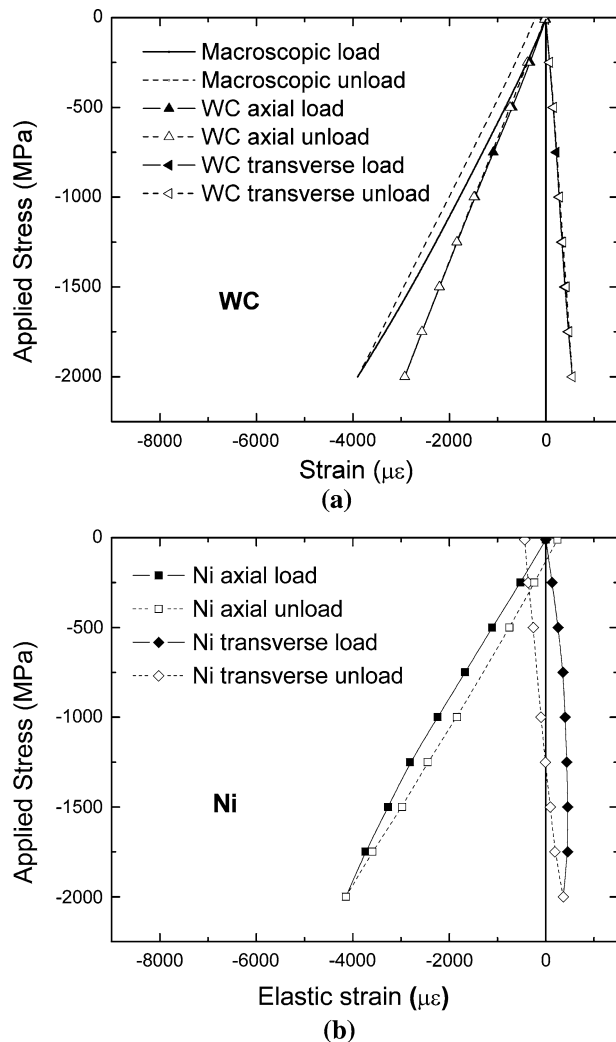


Fig. 1—WC-5 pct Ni load response for the first load cycle: (a) macroscopic and WC and (b) Ni. Loading is represented by closed symbols and solid lines, and unloading by open symbols and dashed lines. The macroscopic axial strain is the total strain measured by an extensometer. The elastic phase strains are measured in the axial and transverse directions by diffraction. The WC strains are determined from the weighted average $(2a + c)/3$. Statistical counting errors in strain are about 30 $\mu\epsilon$ for WC and 45 $\mu\epsilon$ for Ni.

presented in Table IV. The composite values are for total (elastic plus plastic) strain, while the values for WC and Ni are the elastic components only. (Note that the total strain never exceeds 10,000 $\mu\epsilon$ or 1 pct). Upon unloading, there are residual strains. The macroscopic curves have residual compressive strain. The axial plots show residual tension for Ni and residual compression for WC. The transverse plots show residual compression for Ni and residual tension for WC.

In the axial direction, because only elastic strain is measured by diffraction, plastic strain is manifested by a reduction in the rate at which the elastic strain accumulates. In the Ni, the strain accumulation decreases with applied load, indicating yield from the beginning of load. There is a net tensile strain in the axial direction upon unloading for the Ni in all samples. For WC, which is presumed to be elastic throughout, the strain

Table III. Thermal Residual Stresses in the As-Produced WC-Ni Samples Prior to Loading; Stresses in the Ni Phase Are Calculated from the WC Stress Using Force Balance Considerations

Sample	Thermal Residual Stress (MPa)	
	WC	Ni
WC-5 pct Ni	-231 \pm 43	2940 \pm 256
WC-10 pct Ni	-382 \pm 52	2022 \pm 190
WC-20 pct Ni	-764 \pm 88	2005 \pm 207

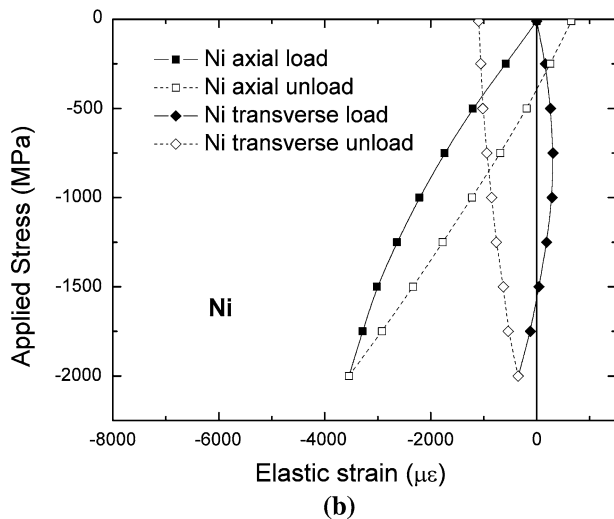
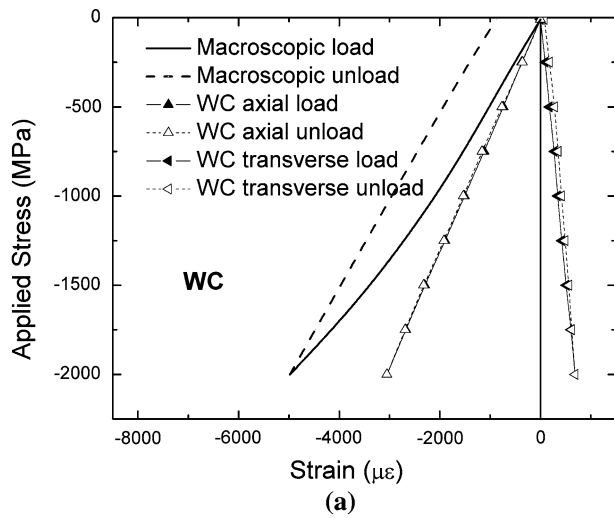


Fig. 2—WC-10 pct Ni load response for the first load cycle: (a) macroscopic and WC and (b) Ni. The same conventions as in Fig. 1 are used. Statistical counting errors in strain are about $30 \mu\epsilon$ for WC and $25 \mu\epsilon$ for Ni.

accumulates in the WC at a faster rate with increasing applied stress. This can only be seen for WC-20 pct Ni (Figure 3(a)). It is due to load transfer from the Ni as it yields.

In the transverse direction, the response for Ni is initially tensile, as expected for the transverse (Poisson) strain response of a sample under uniaxial compression. However, upon increased compressive stress, the accumulation of strain slows and then reverses. Indeed, for the 10 pct Ni and 20 pct Ni samples (Figures 2(b) and 3(b)), it actually becomes compressive relative to the unloaded starting point.

During loading, there are two possible sources of the observed changes: (1) a reduction in the thermal residual microstresses *via* plasticity in the Ni and (2) creation of mechanical microstresses *via* differential flow of the Ni relative to the WC. The applied strain is compressive in the axial direction and tensile in the transverse direction. Thus, it opposes the thermal residual strain in the Ni in the axial direction and adds to it in the transverse direction. The result is tensile flow in the Ni in the

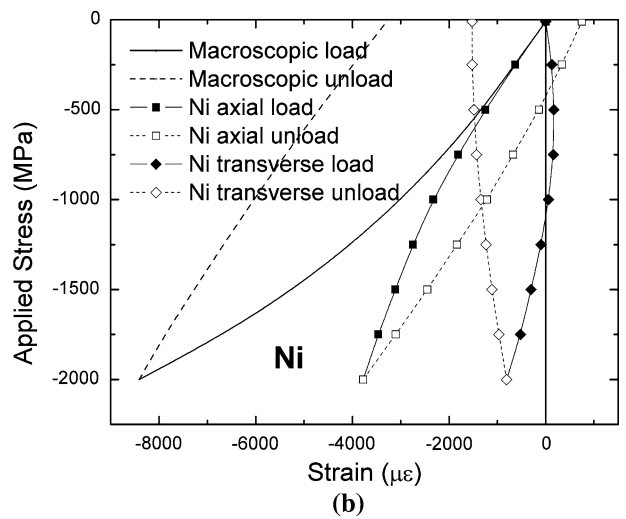
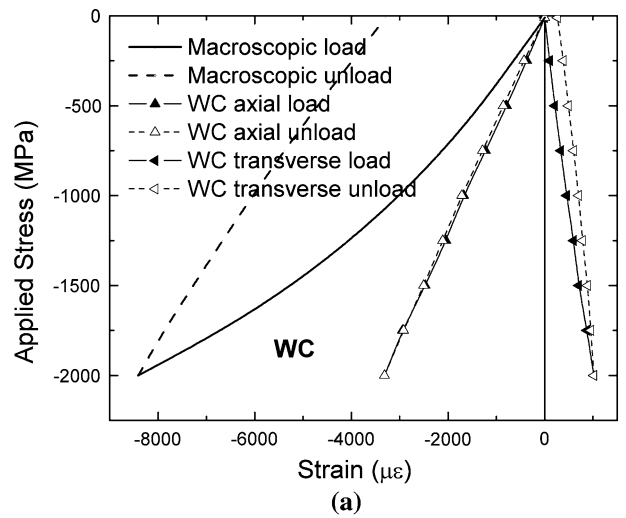


Fig. 3—WC-20 pct Ni load response for the first load cycle: (a) macroscopic and WC and (b) Ni. The same conventions as in Fig. 1 are used. Statistical counting errors in strain are about $50 \mu\epsilon$ for WC and $20 \mu\epsilon$ for Ni.

transverse direction, most likely in those locations in the Ni microstructure with the highest local tensile strains. This results in greater reduction of the TRS in that direction than in the axial direction. It is also possible that, in the axial direction, some flow is possible because of the stress variance, which results in local Ni regions that are under compression.

Table IV. Values for the Total Composite Strain and the Elastic Phase Strains at the Maximum Load Level (-2000 MPa) of the First Load Cycle; the Initial Values Are Given in Table III

Sample	Total Strain ($\mu\epsilon$) Composite	Elastic Phase Strain ($\mu\epsilon$)	
		WC	Ni
WC-5 pct Ni	-3902	-2924	-4141
WC-10 pct Ni	-4981	-3052	-3546
WC-20 pct Ni	-8412	-3316	-3776

This behavior has been previously observed, in a WC-10 wt pct Co cemented carbide similar to those studied here,^[10] in Be-Al composites,^[30] and in WC-17 wt pct (85 Co-15 Ni).^[19] For the WC-10 pct Co, a two-dimensional finite element model that used an interpenetrating microstructure was developed and thermally loaded prior to uniaxial compressive loading. Upon compressive loading, the transverse Co strain in the model showed the beginnings of a sign reversal and reproduced the measured response quite well. The Be-Al composite also had a very fine, but much less angular (spinodal), microstructure in which constraint was significant, as in the present case. Also, the Poisson's ratio for Be is nearly zero (0.03) so that there is little tensile strain generated in the transverse direction under uniaxial compression, creating constraint on the Al. Finite element modeling effectively demonstrated the transverse strain reversal during loading. For the WC-17 wt pct (85 Co-15 Ni), the uniaxial loading created an anisotropic, cylindrically symmetric stress state when it is averaged over the diffracting volume. This is also the case here.

The changes in residual strains relative to the unloaded state in the axial and transverse directions after each load-unload sequence are shown in Table V. They exhibit strong anisotropy; the changes for Ni are tensile in the axial direction and compressive in the transverse direction, while the changes for the WC are much less but of opposite sense, *i.e.*, compressive in the axial direction and tensile in the transverse direction. The cylindrical analysis enables us to account for the anisotropic relaxation of the TRS during the load-unload sequence.

For a cylindrically symmetric stress state, the average axial stress is given by

$$\sigma_{\text{axial}}^i = \frac{1}{s_2^i/2} \left\{ \varepsilon_{\text{axial}}^i - \left[\frac{s_1^i}{s_2^i/2 + 3s_1^i} \right] (2\varepsilon_{\text{trans}}^i + \varepsilon_{\text{axial}}^i) \right\} \quad [4]$$

where σ_{axial}^i is the axial stress of the *i*th phase, and $\varepsilon_{\text{axial}}^i$ and $\varepsilon_{\text{trans}}^i$ are the axial and transverse strains of the *i*th phase. The terms s_1^i and $s_2^i/2$ are the isotropic diffraction elastic constants:

Table VI. Isotropic Diffraction Constants Used for Elastic Stress Calculation

Phase	s_1 (MPa ⁻¹)	$s_2/2$ (MPa ⁻¹)
WC	-0.3539×10^{-6}	1.8214×10^{-6}
Ni	-1.9559×10^{-6}	7.6726×10^{-6}

$$s_1 = -\frac{\nu}{E} \quad [5]$$

$$s_2/2 = \frac{1 + \nu}{E}$$

where E is Young's modulus and ν is Poisson's ratio. The values of s_1 and $s_2/2$ used for the WC and Ni phases are given in Table VI. The transverse stress is given by

$$\sigma_{\text{trans}}^i = \frac{1}{s_2^i/2} \left\{ \varepsilon_{\text{trans}}^i - \left[\frac{s_1^i}{s_2^i/2 + 3s_1^i} \right] (2\varepsilon_{\text{trans}}^i + \varepsilon_{\text{axial}}^i) \right\} \quad [6]$$

Our measurement amounts to an application of the *two-tilt method*,^[2] for which the two tilts or sample orientations are 0 deg (diffraction vector parallel to cylinder axis of the sample) and 90 deg (diffraction vector normal to the cylinder axis of sample). The stresses after all loading cycles are shown in Table VII.

Load fractions carried by the WC phase can be computed from Eq. [4]. The load fractions carried by the WC are approximately 0.96, 0.91, and 0.84 for the 5 pct Ni, 10 pct Ni, and 20 pct Ni samples, respectively. That is, the values are essentially constant as the applied stress varies and do not change from one load cycle to the next. A constant value of load fraction means that, even though there is flow in the Ni, little shift in load from Ni to WC occurs during the loading. This is reasonable due to the high WC content, high WC stiffness relative to Ni, and constraint effects.

C. Phase-Specific Elastic Stress–Elastic Strain Curves

Because we have measured in the axial and transverse directions over a range of stress levels, we can use Eqs.

Table V. Residual Strains of the WC-Ni Samples at the End of Each Load Cycle; All Values Are Relative to the Initial Cell Parameters Obtained Prior to Loading; for the WC Phase, the Strains Are Obtained by the Weighted Average, $(2a + c)/3$, of the Strains in the Axial Directions of the Hexagonal Cell

Sample	Cycle	Axial Composite Strain Change ($\mu\epsilon$)	Phase-Specific Strain Changes ($\mu\epsilon$)			
			Axial		Transverse	
			WC	Ni	WC	Ni
5 pct Ni	1	-231 ± 24	-23 ± 18	242 ± 44	-4 ± 13	-439 ± 28
	2	-242 ± 23	-8 ± 18	343 ± 44	-2 ± 13	-504 ± 28
	3	-250 ± 23	-44 ± 18	354 ± 44	-2 ± 13	-568 ± 28
10 pct Ni	1	-877 ± 16	-2 ± 19	656 ± 22	78 ± 17	-1093 ± 21
	2	-942 ± 16	0 ± 19	713 ± 22	89 ± 17	-1203 ± 21
	3	-972 ± 16	-17 ± 19	756 ± 22	89 ± 17	-1267 ± 21
20 pct Ni	1	-3292 ± 23	3 ± 32	748 ± 17	268 ± 25	-1523 ± 15
	2	-3521 ± 24	-20 ± 32	836 ± 17	282 ± 25	-1633 ± 15
	3	-3640 ± 25	25 ± 32	872 ± 18	296 ± 25	-1685 ± 15

Table VII. Residual Stresses in the WC-Ni Samples after All Loading Cycles

Sample	Initial TRS (MPa)		Axial (MPa)		Transverse (MPa)	
	WC	Ni	WC	Ni	WC	Ni
WC-5 pct Ni	-231 ± 43	2940 ± 256	-256 ± 47	2931 ± 599	-227 ± 55	2798 ± 600
WC-10 pct Ni	-382 ± 52	2022 ± 190	-374 ± 56	1976 ± 271	-321 ± 60	1664 ± 271
WC-20 pct Ni	-764 ± 88	2005 ± 207	-614 ± 91	1855 ± 168	-422 ± 90	1460 ± 168

[4] and [6] to construct elastic stress-strain curves for each phase from the measured strain. In this section, we focus on the 20 pct sample because it shows the effects most clearly. Figure 4 shows the phase stress vs the elastic phase strain for the WC-20 pct Ni sample during the first load-unload cycle. The plots are relative to the unloaded state, which is set at zero stress and strain, *i.e.*,

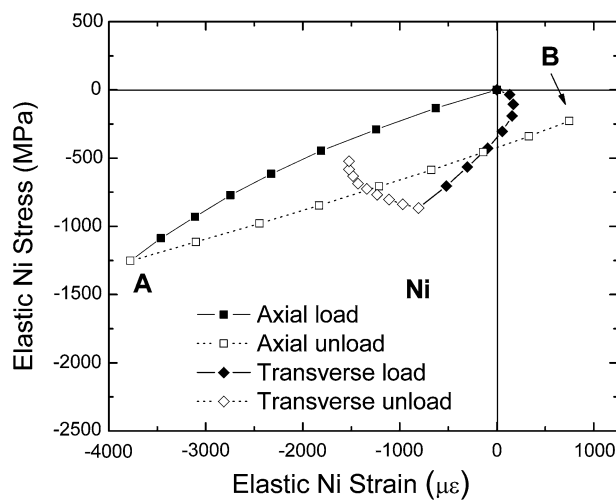
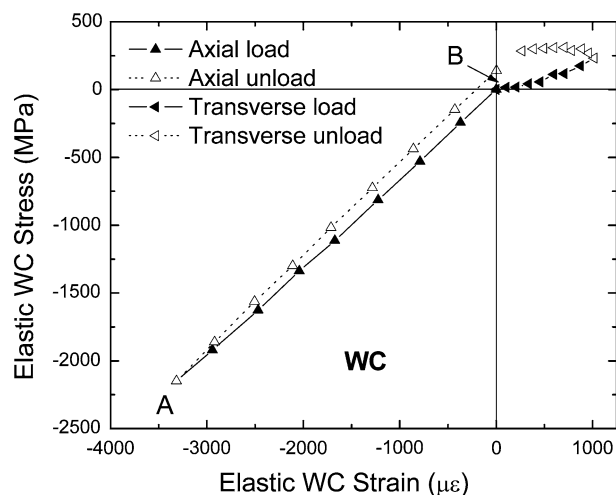


Fig. 4—Phase elastic stress vs phase elastic strain for (a) WC and (b) Ni in the WC-20 pct Ni sample. The first load-unload cycle is shown. Point A indicates the compressive phase stress at the maximum applied compressive load. Point B indicates the change in residual stress in the phases as a result of loading. The statistical counting errors for stresses are about 38 MPa for WC and 6 MPa for Ni.

the preexisting thermal residual stress is not included. The successive data points are in increments of 250 MPa of applied stress. These plots reveal changes in both stress and strain in each phase due to plastic flow in the Ni.

In the axial direction, the applied strain is compressive for both phases during loading (points A in Figures 4(a) and (b)). There are changes in the residual stresses in both phases as a result of the loading cycle due to the two sources of change cited previously. Source (1) reduces the initial TRS through flow of the Ni. The local Ni flow upon loading is expected to decrease the magnitudes of the pre-existing TRS in both phases. Thus, in the axial direction, the change is negative (compressive) in the Ni and positive (tensile) in the WC (points B in Figures 4(a) and (b)). Source (2) creates microstresses *via* differential flow of the Ni relative to the WC. In the axial direction, this is expected to create a tensile stress in the Ni and a compressive stress in the WC. Thus, the two sources lead to opposing effects in each phase.

In the transverse direction, the Poisson strain due to the applied axial load is tensile for both phases. In this case, (1) the Ni flow again causes a decrease in the magnitudes of the thermal residual stresses and strains and (2) a compressive residual stress and strain is created in the Ni upon release of the applied load, and a counterbalancing tension is established in the WC. In this case, it is significant that the Poisson tensile strain acts in the same sense as the pre-existing tensile thermal residual strain in the Ni, *i.e.*, that the mechanism for reduction of the TRS is enhanced in the transverse direction. This suggests that the observed changes in residual stress would be greatest in the transverse direction.

A summary of the signs of the changes in residual stresses induced by Ni flow is shown in Table VIII. The measured changes confirm that they are greatest in the

Table VIII. Predicted Signs of the Changes in Residual Stresses Resulting from Ni Flow for WC-20 Pct Ni Due to (1) Differential Mechanical Flow and (2) Thermal Residual Stress Relaxation; the Model Assumes That Ni is Elastic-Plastic and WC is Elastic; Signs of the Initial Thermal Residual Stresses Are in Parentheses

Changes in Residual Stress	Axial		Transverse	
	WC (-)	Ni (+)	WC (-)	Ni (+)
Predicted mechanical	-	+	+	-
Predicted thermal	+	-	+	-
Measured changes	+150	-150	+342	-545

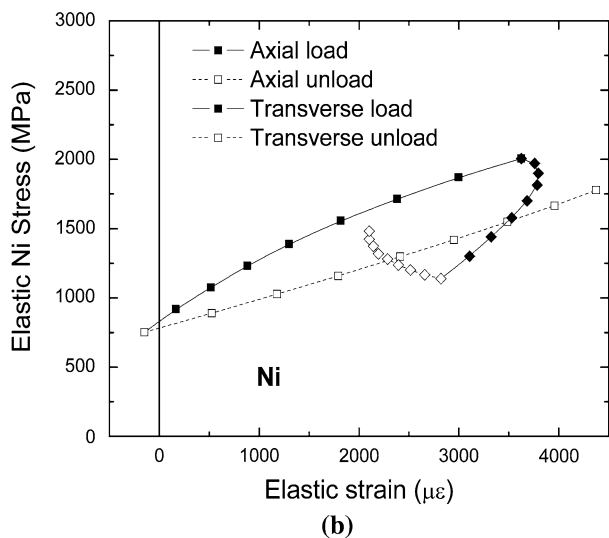
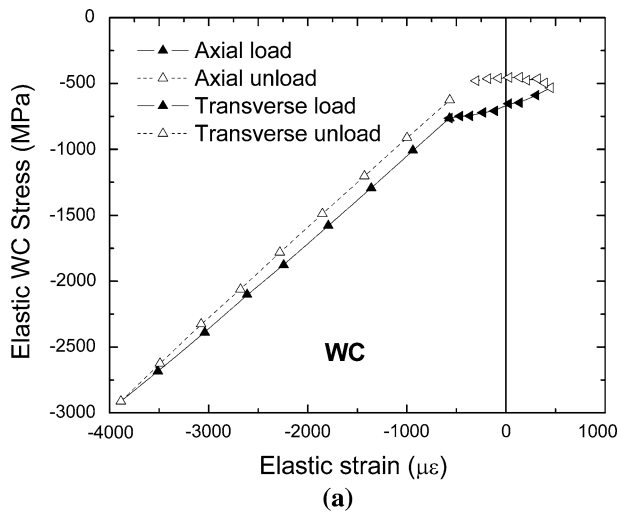


Fig. 5—The total (residual plus applied) elastic phase elastic stress vs the total elastic phase elastic strain for (a) WC and (b) Ni in the WC-20 pct Ni sample. The first load-unload cycle is shown. The errors in elastic strain are about $50 \mu\epsilon$ for WC and $20 \mu\epsilon$ for Ni. The errors in stress are dominated by the errors in the initial TRS, which are about 90 MPa for WC and 210 MPa for Ni.

transverse direction. Finally, it is possible to add in the initial thermal residual stresses to obtain a fuller picture of the stress-strain response in the phases (Figure 5).

D. Multiple Cycles

Results for all three cycles, for the WC-20 pct Ni sample, are shown in Figure 6. The macroscopic and Ni phase curves are shown in Figures 6(a) and (b), respectively. There are three primary features. First, there is a wide hysteresis loop after the first load-unload cycle that closes considerably after the subsequent cycles. Second, residual strain continues to change with additional cycles, as shown in Table V. This is clearest for Ni, but visible for the transverse strains in WC for the 10 and 20 pct samples. The accumulation of residual strain may continue for many cycles, though in smaller and smaller increments.^[29] Measurements to 100 cycles will

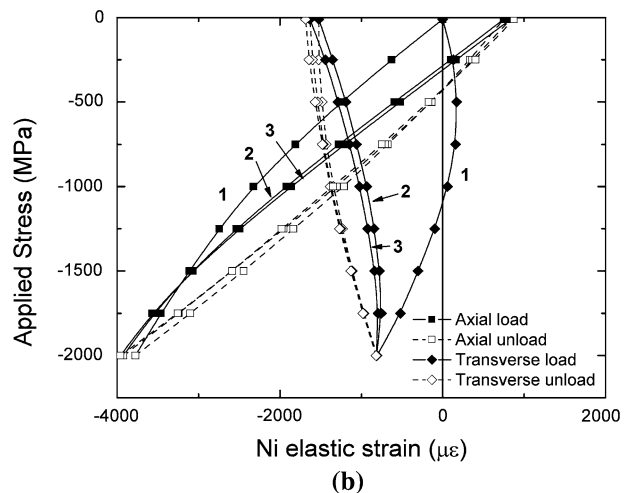
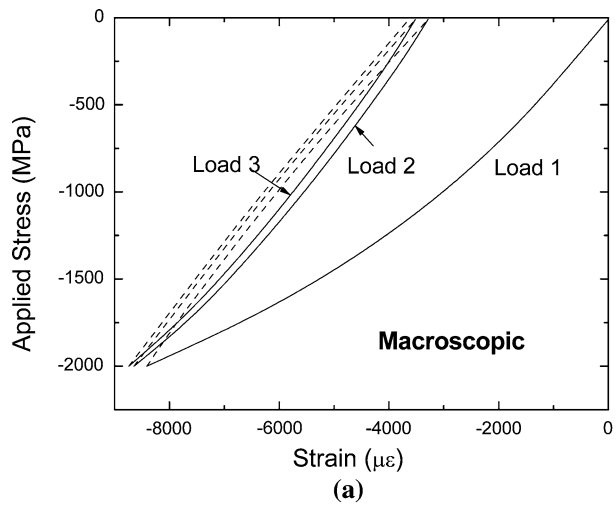


Fig. 6—Three complete loading cycles for the WC-20 pct Ni sample: (a) macroscopic and (b) Ni responses are shown. Loading is represented by closed symbols and solid lines, and unloading is represented by open symbols and dashed lines. The macroscopic strain is the total axial strain measured by an extensometer, and the Ni strains are elastic and measured in the axial and transverse directions by diffraction.

be reported in the future. Third, neither the loading nor the unloading curves become linear; curvature persists, although it decreases as the number of cycles increases. This is particularly clear for the macroscopic response and the Ni phase. The curvature is attributed to binder yield in localized areas throughout the microstructure, areas that comprise a very small fraction of the binder volume so that the volume-averaged change in residual strain is small. In addition, unloading curvature may include some component of Bauschinger effect in yielded binder regions where most of the unload cycle corresponds to a reversal in the local shear strain.

Does the process of local flow and net reduction in residual stress continue indefinitely or fade out rather quickly? Is the TRS necessary for the process to occur? Does the process end if the initial TRS is eliminated by the accumulating local plastic flow? Further data to address these issues have been taken and will be reported. The process appears to continue for many

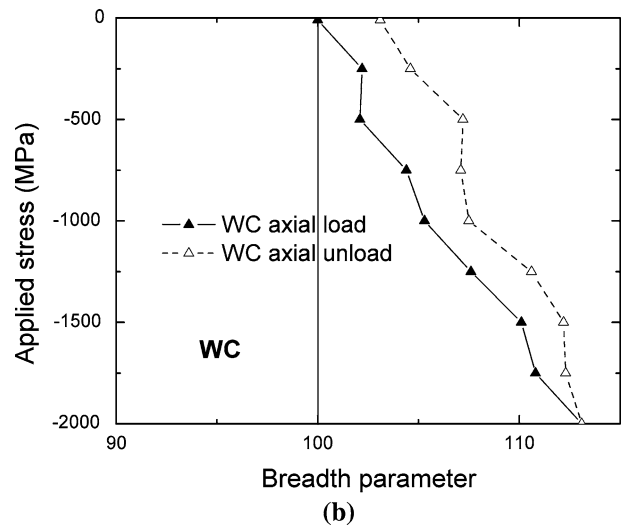
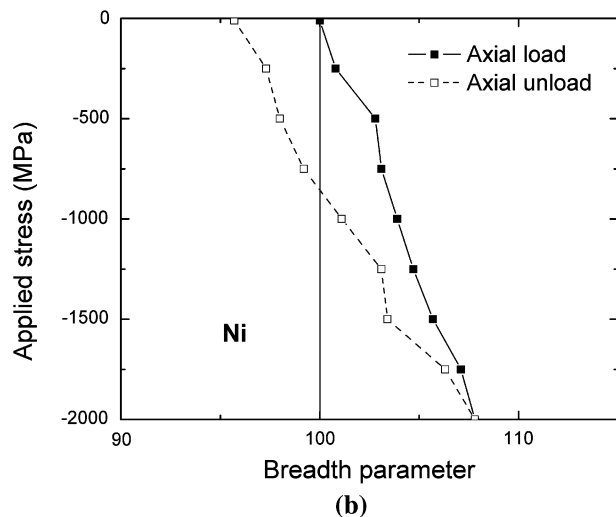
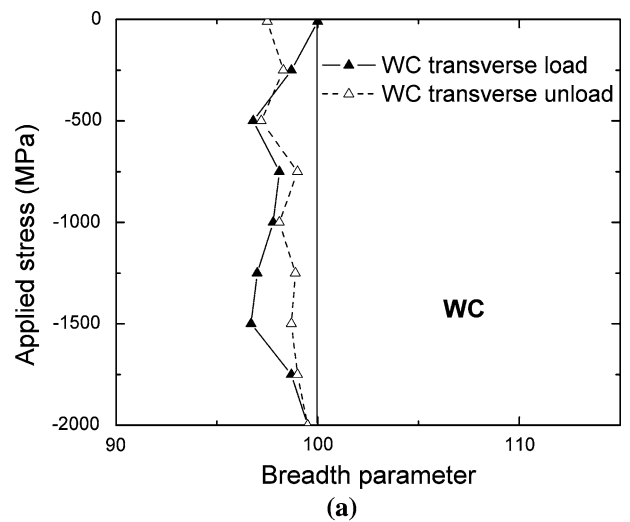
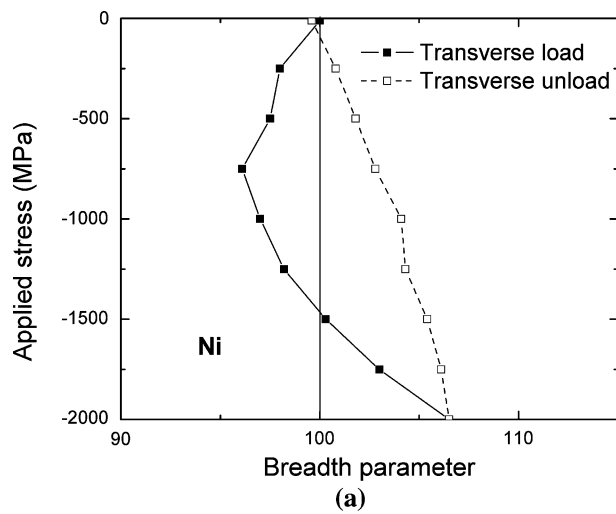


Fig. 7—Peak breadths during the first load cycle for the Ni in the (a) transverse and (b) axial directions for the WC-20 pct Ni sample. The data are the average of the 111, 200, and 311 diffraction peaks. Closed symbols and solid lines are the load segment, and open symbols and dotted lines are the unload segment of the cycle. The fitting error for these values is less than 1.0 in breadth parameter units.

Fig. 8—Peak breadths during the first load cycle for WC in the (a) transverse and (b) axial directions for the WC-20 pct Ni sample. The data are the average of the 101 and 201 peaks. Closed symbols and solid lines are the load segment, and open symbols and dotted lines are the unload segment of the cycle. The fitting errors for these values are about 1.0 in breadth parameter units.

cycles, though the rate of relaxation slows. However, the proposed process does not necessarily depend on the presence of an initial TRS. It may occur independently of it and even create a reverse microstress state due to the local Ni flow.

E. Strain Distribution

Peak breadths during the first load cycle for Ni and WC in the axial and transverse directions for the WC-20 pct Ni sample are shown in Figures 7 and 8, respectively. The Ni plots are averages of the 111, 200, and 311 peaks; the WC plots are averages of the 101 and 201 peaks. For both phases, the trend for each hkl was consistent with the averages shown. The breadth parameters are based on the time-of-flight peak widths in microseconds and are normalized with respect to the breadths at the start of the loading sequence for each peak used. The initial

breadths are arbitrarily set to 100. Instrumental breadths for the same geometry and sample sizes were not available, so the breadths shown are not corrected for instrumental broadening. In general, peak breadths can be affected by (1) elastic strain distribution in the diffracting volume, (2) dislocations due to cold work, and (3) size effects due to very small diffracting regions. In the present case, as in previous work in such systems,^[11–13,15,24,31] the primary source of changes in peak breadths is the first one. A hallmark of effect (1) is that it can be reversible, as a result of reverse changes in temperature or applied load. In general, both the mean strain (stress) and strain (stress) variance are affected.

For Ni, the peak breadths initially decrease in the transverse direction (Figure 7(a)) as the magnitude of the applied load increases. This is consistent with the initiation of plastic flow in the transverse direction in the Ni in regions of high local tension. Such flow would

reduce the *range* of elastic strain in the diffracting volume by lowering strains at the tensile end of the distribution, creating a *decrease* in the elastic strain *variance* in the transverse direction. At an applied stress of about -750 MPa, the peak widths stop sharpening and start to broaden. At the maximum compressive load, -2000 MPa, they are broader than when they started. This suggests that, initially, there are regions of local tensile strain that readily flow but that, once triggered, it is harder for the system to yield locally. The result is that the system becomes more elastic, increasing the strain variance. The change in the *mean* strain during loading is essentially the opposite of the change in strain variance. Comparison of Figures 4(b) and 5(b) with Figure 7(a) shows that the mean elastic strain initially increases, then decreases, while the strain variance, as described previously, does the opposite. However, upon unloading, both the mean phase strain and the strain variance decrease in the transverse direction.

In the axial direction (Figure 7(b)), the Ni peak breadths steadily broaden during loading even though the applied strain opposes the pre-existing mean thermal residual strain. Thus, while the mean axial strain is decreasing, the strain variance is increasing. This is partly an elastic constraint effect because, during *unloading*, the peaks sharpen again. When unloading is complete, the peak breadths are sharper than at the beginning due to the plastic flow occurring primarily in the transverse direction and the consequent reduction in the extremes of the strain distribution.

For WC in the transverse direction (Figure 8(a)), statistically insignificant changes occur. Figures 4(a) and 5(a) show that the changes in mean transverse strain in WC are also small during loading and unloading. This is a case where the modulus of the material is so high and the mean stresses so low that the effect on strain variance is correspondingly small. In this sense, the changes in mean strain and strain variance are in agreement. However, for WC in the axial direction, the peak breadths increase with the applied compressive stress. As shown in Figures 4(a) and 5(a), the axial compression in the WC phase reaches very high *mean* values that lead to an increase of the strain variance in the elastic WC phase. As the sample is unloaded, the breadth decreases; however, there is a residual broadening. Two possible sources are proposed. The first is due to the action of the adjacent Ni. The decrease in local residual tensile strain in the Ni, due to plastic flow, causes local contraction of Ni, which applies added compression to the neighboring WC, leading to an increase in strain variance in WC even though the mean strain decreases. Another possibility is that the local variability of deformation strains is larger than that for thermal strains.

The transverse peak breadths for Ni through all three load cycles are shown in Figure 9. The general character of each load-unload loop is the same. The breadths initially decrease and then they increase. Upon final unloading, there appears to be a net decrease in peak breadth. A small net decrease in peak breadth is evident. However, the width of the hysteresis loop narrows as the

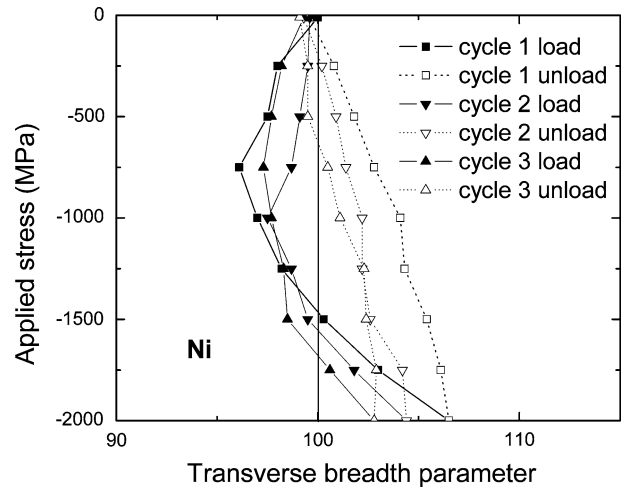


Fig. 9—Peak breadths for the first, second, and third load-unload cycles for Ni in the transverse direction for the WC-20 pct Ni sample. The data are the average of the 111, 200, and 311 peaks. Closed symbols and solid lines are the load segment, and open symbols and dotted lines are the unload segment of the cycles. The fitting errors are less than 1.0 in breadth parameter units.

number of cycles increases. This indicates that the same mechanism continues to operate.

F. Toughness

The results suggest a mechanism for the unusually high toughness of cemented carbides. Plasticity of the composite as a whole begins from the earliest stages of applied strain, as evidenced in the continuously curved macroscopic stress-strain curves. Application of the modified law of mixtures for strains, which is valid at low total strains, reveals the extent of the plasticity.^[32] The strain is given by

$$\varepsilon_{\text{axial}}^c = (1 - f)\varepsilon_{\text{axial}}^{\text{WC}} + f\varepsilon_{\text{axial}}^{\text{Ni}} \quad [7]$$

where $\varepsilon_{\text{axial}}^c$ is the total composite strain in the axial direction, $\varepsilon_{\text{axial}}^{\text{WC}}$ and $\varepsilon_{\text{axial}}^{\text{Ni}}$ are the total strains in the WC and Ni, and f is the volume fraction of Ni. This relation is valid for small strains and in the presence of plasticity. Because the diffraction measurements of the phase strains do not include the plastic contribution, and the WC is assumed to be elastic in this region of strain, the discrepancy between the macroscopic extensometer values and the measured values of the elastic strains for the phases is the plastic strain for the Ni. Figure 10 shows the modified law of the mixtures line with the actual macroscopic extensometer (composite) stress-strain response for WC-20 pct Ni. The early onset of plastic deformation can be explained by localized yielding of the binder on a microscopic level in the extremes of the shear stress distribution, where the sense of the applied shear strain is additive. The aggregation of local plastic binder deformations results in the plastic behavior of the composite as a whole. This yielding acts over the entire volume of the externally loaded composite and provides a mechanism for the absorption and redistribution of elastic strain

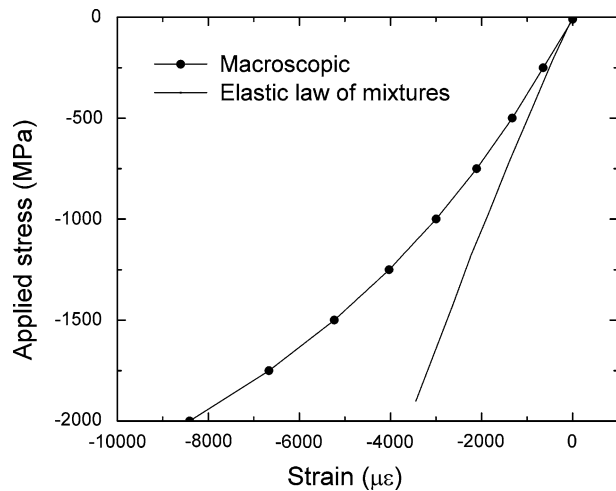


Fig. 10—Comparison of the axial response of WC-20 pct Ni during the first load cycle with the law of mixtures elastic stress-strain curve.

energy around defects, which is the predominant means of toughening in metals. The nature of this complex yielding behavior, including distribution and magnitudes of microstrains as well as the macroscopic response, has been modeled for an idealized microstructure by finite element methods, with good agreement.^[10,15]

The continuum treatment of toughness in ductile materials that models crack stability in terms of elastic and plastic zones is not applicable to composites with no proper elastic-plastic transition. Moreover, the pronounced anisotropy of the strain/yield/TRS responses shown in these findings may have significant implications for the development of elastic strain fields around defects in externally loaded composites. For the present, simpler case of a uniformly loaded cylinder, the yielding can be summarized in terms of principal strains. The Ni is under a large mean residual tensile thermal strain, due to cooling from high temperatures, that interacts additively with the applied uniaxial compression. In the axial direction, the result is decreasing axial tensile strain, while, in the transverse direction, the strains are increasing, resulting in disproportionate plastic strain in the transverse direction. The process continues for many load cycles, because (1) the initial TRS is lowered very slowly after the initial load cycle and (2) the stress-strain curves continue to be curved upon further loading.

IV. CONCLUSIONS

The elastic load response of WC-Ni cemented carbides was measured through three compressive loading cycles using *in-situ* neutron diffraction. The initial thermal residual stresses and final residual stresses were measured, as well as the mean residual strains and stresses and their variances, throughout the loading cycles. The interaction of the externally applied compressive macrostress with the thermal residual micro-

stress is complex. The fundamental conclusion is that extensive discrete microscale yield events distributed throughout the sample give rise to macroscale yielding, which begins with the initial application of external stress. This plastic strain response is an elastic strain energy absorption mechanism and, at least in part, accounts for the unusually high toughness of cemented carbides.

The macroscopic and diffraction data indicate that plastic flow occurs from the earliest loads. The largest amount of plastic flow, which essentially occurs only in the binder, takes place during the first cycle and increases incrementally thereafter. Anisotropic relaxation of the initial thermal residual stresses in the binder phase is observed, with more relaxation occurring in the transverse direction than in the axial direction. There appear to be two mechanisms involved, both of which result from flow of the Ni: plastic relaxation and the creation of opposing residual stress *via* differential flow of the Ni relative to the WC. Flow is believed to be localized at the extremes of the shear stress distribution where the sense of applied shear strain is additive.

ACKNOWLEDGMENTS

The authors acknowledge useful insights provided by Dr. D. Mari, EPFL (Lausanne, Switzerland). This work was supported by ReedHycalog through a grant to the University of Missouri. Funding for SMARTS and the operation of Lujan Center, a national user facility, was provided by the United States Department of Energy, Office of Basic Energy Sciences, under Contract No. W-7405-ENG-36.

REFERENCES

1. G.S. Upadhyaya: *Cemented Tungsten Carbides: Production, Properties, and Testing*, Noyes Publications, Westwood, NJ, 1998.
2. H.E. Exner and J. Gurland: *Powder Metall.*, 1970, vol. 13, pp. 13–31.
3. J.L. Chermant and F. Osterstock: *J. Mater. Sci.*, 1976, vol. 11, pp. 1939–57.
4. H.E. Exner: *Int. Met. Rev.*, 1979, vol. 24, pp. 149–73.
5. L.S. Sigl and H.E. Exner: *Metall. Trans. A*, 1987, vol. 18A, pp. 1299–308.
6. B. Roebuck and E.A. Almond: *Int. Met. Rev.*, 1988, vol. 33, pp. 90–110.
7. J. Gurland: *Int. Met. Rev.*, 1988, vol. 33, pp. 151–66.
8. L.S. Sigl and F.F. Fischmeister: *Acta Metall.*, 1988, vol. 36, pp. 887–97.
9. K.S. Ravichandran: *Acta Metall. Mater.*, 1994, vol. 42, pp. 143–50.
10. V. Livescu, B. Clausen, J.W. Paggett, A.D. Krawitz, E.F. Drake, and M.A.M. Bourke: *Mater. Sci. Eng.*, 2005, vol. A399, pp. 134–40.
11. A.D. Krawitz, D.G. Reichel, and R.L. Hitterman: *Mater. Sci. Eng.*, 1989, vol. A119, pp. 127–34.
12. A.D. Krawitz, M.L. Crapenhof, D.G. Reichel, and R. Warren: *Mater. Sci. Eng.*, 1988, vols. A105–A106, pp. 275–81.
13. A.D. Krawitz, R. Roberts, and J. Faber: in *Science of Hard Materials*, Institute of Physics Conf. Series No. 75, Adam Hilger Ltd., 1984, pp. 577–89.

14. K. Seol, A.D. Krawitz, J.W. Richardson, and C.M. Weisbrook: *Mater. Sci. Eng.*, 2005, vol. A398, pp. 15–21.
15. C.M. Weisbrook and A.D. Krawitz: *Mater. Sci. Eng.*, 1996, vol. A209, pp. 318–28.
16. M.A.M. Bourke, D. Dunand, and E. Ustundag: *Appl. Phys. A (Mater. Sci. Process.)*, 2002, vol. A74, p. S1707.
17. H.M. Rietveld: *J. Appl. Crystallogr.*, 1969, vol. 2, part 2, pp. 65–71.
18. D.A. Witte, A.D. Krawitz, R.A. Winholtz, R.R. Berliner, and M. Popovici: *J. Neutron Res.*, 1998, vol. 6, pp. 217–32.
19. K. Seol and A.D. Krawitz: *Mater. Sci. Eng.*, 1990, vol. A127, pp. 1–5.
20. I.C. Noyan and J.B. Cohen: *Residual Stress; Measurement by Diffraction and Interpretation*, Springer-Verlag, New York, NY, 1987.
21. A.D. Krawitz: *Introduction to Diffraction in Materials Science and Engineering*, John Wiley and Sons, New York, NY, 2001.
22. T. Gnäupel-Herold, P.C. Brand, and H.J. Prask: *J. Appl. Cryst.*, 1998, vol. 31, pp. 929–35.
23. G. Simmons and H. Wang: *Single Crystal Elastic Constants and Calculated Aggregate Properties: A Handbook*, 2nd ed., MIT Press, Cambridge, MA, 1971.
24. D.L. Coats and A.D. Krawitz: *Mater. Sci. Eng.*, 2003, vol. A359, pp. 338–42.
25. T. Christman, A. Needleman, and S. Suresh: *Acta Metall.*, 1989, vol. 37, pp. 3029–50.
26. D.C. Drucker: *J. Mater.*, 1966, vol. 1, p. 873.
27. R.P. Felgar and J.D. Lubahn: *Proc. ASTM*, 1957, vol. 57, pp. 770–88.
28. B.O. Jaensson: *Mater. Sci. Eng.*, 1972, vol. 9, pp. 339–46.
29. E.F. Drake and A.D. Krawitz: *Metall. Trans. A*, 1981, vol. 12A, pp. 505–13.
30. D.H. Carter and M.A.M. Bourke: *Acta Metall.*, 2000, vol. 48, pp. 2885–2900.
31. A.D. Krawitz, R.A. Winholtz, and C.M. Weisbrook: *Mater. Sci. Eng.*, 1996, vol. A206, pp. 176–82.
32. K. Cho and J. Gurland: *Metall. Trans. A*, 1988, vol. 19A, pp. 2027–40.